CHAPTER 4

QUANTUM DOTS: SYNTHESIS, CHARACTERIZATION AND APPLICATIONS

QUANTUM DOTS: SYNTHESIS, CHARACTERIZATION, AND APPLICATIONS

4.1 Introduction

Fluorescent quantum dots (QDs) or semiconductor nanocrystals were introduced in the biomedical field in the year of 1998 [1]. QDs possess several advantages over the conventional organic fluorophores like broad absorption spectra, high photostability, large extinction coefficient and tunable emission wavelengths. In the past decade, fluorescent quantum dots (QDs) have attracted considerable interest in the scientific community due to their interesting size dependent properties arising from quantum confinement effect, leading to many promising applications in biomedical fields [2-8]. Two different classes of fluorescent QDs; colloidal fluorescent and carbonaceous QDs, have fuelled up intensive research for tuning its properties suitable for biomedical applications. Colloidal fluorescent QDs exhibiting a long fluorescence life time (Ű > 10 ns) are suitable for various biomedical applications [9, 10]. A fluorescent material with a short fluorescence life time may suffer interferences from some biological molecules that have short fluorescence lifetimes and hence are not appropriate for biomedical applications. Some of the important parameters of QDs like a long life time, hydrophilicity and biocompatibility are crucial for its applicability in the different biomedical field [11, 12].

In the objective of the thesis in **chapter 1**, we have proposed about the development of multimodal hybrid nanosystems where it is required to integrate the magnetic and fluorescent components into a single system. The development of thioglycolic acid (TGA) capped magnetic FePt by polyol process was discussed in **section C** of **Chapter 3**. Aforementioned TGA capped FePt was chosen for the development of multimodal hybrid nanosystems because the negative surface charge of FePt will be capable of binding to the positively charged Cd ions. In this chapter, we have developed different Cd-based QDs through a polyol process with optimized precursor ratio and reaction temperature for achieving high fluorescence efficiency. The similar synthesis protocol

will be used for the synthesis of pristine QDs for development of the multimodal hybrid nanosystems, which will be described in next chapter.

This chapter is divided into two sections- A and B based on the sources used i.e. Te/Se and S, for the synthesis of different types of QDs. In section A, Te and Se precursors were used for the development of glutathione (GSH) capped CdTe and CdSe QDs whereas in section B the capping agent GSH was used as a sulfur source as well as capping agent for the development of glutathione (GSH) capped CdS QDs.

4.2 Material and Methods

This section enlists the materials used and the procedure adopted for the synthesis of CdTe, CdSe, and CdS QDs. A polyol process is used for the synthesis of aforementioned QDs.

Materials used for the development of CdTe, CdSe and CdS QDs

For the synthesis and purification procedure of the pristine CdTe, CdSe, and CdS QDs, analytical grade materials were used as received without purification. Cadmium chloride monohydrate ($CdCl_2.H_2O$ 99%) was used as Cd source whereas the sodium tellurite (Na_2TeO_3, 100 mesh, 99%) from Sigma-Aldrich was used as tellurium source. Selenium powder (Se, 100 mesh, 99.99%) from Sigma-Aldrich was used as a selenium source in CdSe nanosystem. Glutathione (GSH, $C_{10}H_{17}N_3O_6S$, 99%) from Sisco Research Laboratory (SRL) was used as the capping agent for aforementioned QDs as well as sulfur source for the formation of CdS QDs. De-ionized water (Type I) was used for purification, characterization, and experimental processes.

Section-A

4.3 Synthesis of CdTe and CdSe fluorescent quantum dots:

A novel one-pot synthesis was adopted for the development of the hydrophilic CdX (X= Te or Se) fluorescent QDs, where glutathione was used as the capping agent. The CdTe and CdSe QDs were developed by two separate reactions. A schematic diagram (**figure 4.1)** represents the synthesis steps involved in the synthesis process of these two QD

systems. In the synthesis process, the nucleation of CdTe or CdSe starts after addition of Te or Se source at the temperature 140 °C, which was followed by growth and capping in between 150 ï 230 °C.

The synthesis process of CdTe and CdSe was similar, but it was synthesized independently. Initially, the solution of Cd and Se/Te source was prepared by dissolving 2.5 mmol $CdCl_2.H_2O$ and 0.5 mmol of Na_2TeO_3/Se powder in 5 ml of ethylene glycol.

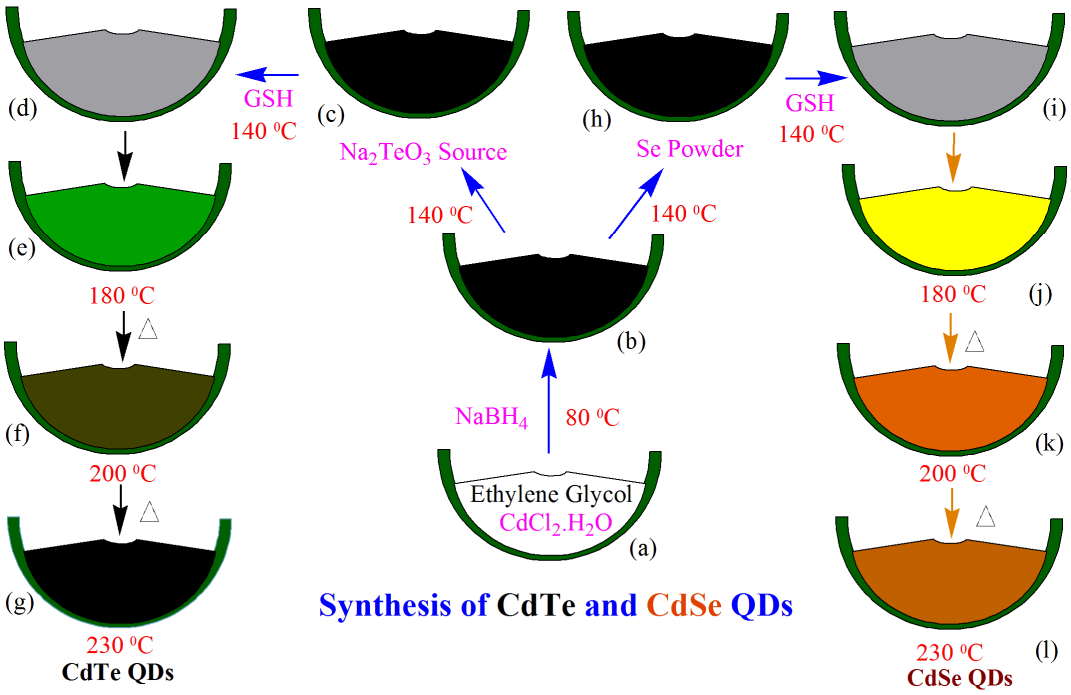

Figure 4.1 Schematic diagram illustrating steps involved and changes in the colour of reaction liquid with temperature variation during the synthesis of CdTe and CdSe fluorescent quantum dots

A 100 mL three-necked round bottom flask, containing 20 ml of ethylene glycol was placed over the hot plate with a magnetic bar inside for stirring. After that, 5 mL of 5 mmol $CdCl_2.H_2O$ solution was added in the reaction vessel at room temperature. At this stage, the colour of reaction liquid is white (**refer figure 4.1 (a)**). Now, the temperature of the flask was increased using a hot plate in an open atmosphere at the rate of 1 °C per minute. When the temperature rises up to 80 °C, 4 mmol $NaBH_4$ was added into the flask (**refer figure 4.1 (b)**). After addition of reducing agent, the colour of reaction

liquid turns into black may be due to the reduction of Cd compound. Till this stage, the reaction condition for the synthesis of both CdTe and CdSe QDs was same. The molar ratio of Cd with Te or Se was kept to 5:1 in both (CdTe and CdSe) reaction synthesis procedure.

For the synthesis of CdTe QDs, Na_2O_3Te (1 mmol in 5 ml of ethylene glycol) was added dropwise into the reaction vessel at 140 ℃ (**refer figure 4.1 (c)**). At this stage, the colour of the reaction medium changes from black to grey. After 15 minutes, at the same temperature, 0.25 mmol glutathione was injected into the reaction vessel (**refer figure 4.1 (d)**). In the next step, the temperature was increased up to 230 ℃ at the rate of 1 ℃/min. At the temperatures of 180, 200 and 230 ℃, the vessel liquid colour changes from grey to light green, dark green and black colour respectively (**refer figure 4.1 (e, f and g)**). After attaining a temperature of 230 ℃, the heating process was stopped and allowed to cool down to room temperature for purification.

Likewise, for the synthesis of CdSe QDs, Se powder solution (1 mmol in 5 ml of ethylene glycol) was added dropwise into the reaction vessel at 140 ℃ (**refer figure 4.1 (h)**). After the addition of Se precursor, the colour of reaction medium changes from black to grey. After 15 minutes, at the same temperature, 0.25 mmol glutathione was added in the reaction vessel and the temperature of the reaction vessel was increased at the rate of 1 ℃/min up to 230 ℃ (**refer figure 4.1 (i)**). At temperature 180, 200 and 230 ℃, the vessel liquid colour changes from grey to light yellow, light brown and dark brown colour respectively (**refer figure 4.1 (j, k and l)**). After attaining a temperature of 230 ℃, the heating process was stopped and allowed to cool down to room temperature for purification.

Purification steps were also same for both synthesis processes. The precipitate was separated from the reaction mixture by centrifugation and washed three times using hexane, isopropyl alcohol and methanol to remove the residual surfactants. The purified masses obtained in the case of CdTe and CdSe were black and dark brown respectively. These were used for further characterization. The same reaction condition was applied for the synthesis of CdTe and CdSe fluorescent quantum dots on FePt MNPs for the development of core/shell multimodal hybrid nanosystem FePt@CdTe and FePt@CdSe.

4.4 Characterization

The synthesized QDs were characterized using several techniques for in-depth understanding of properties.

4.4.1 Results and discussion

Microstructural characterization of quantum dots was carried out using x-ray diffraction (XRD), transmission electron microscopy (TEM) and selected area electron diffraction (SAED) pattern analysis.

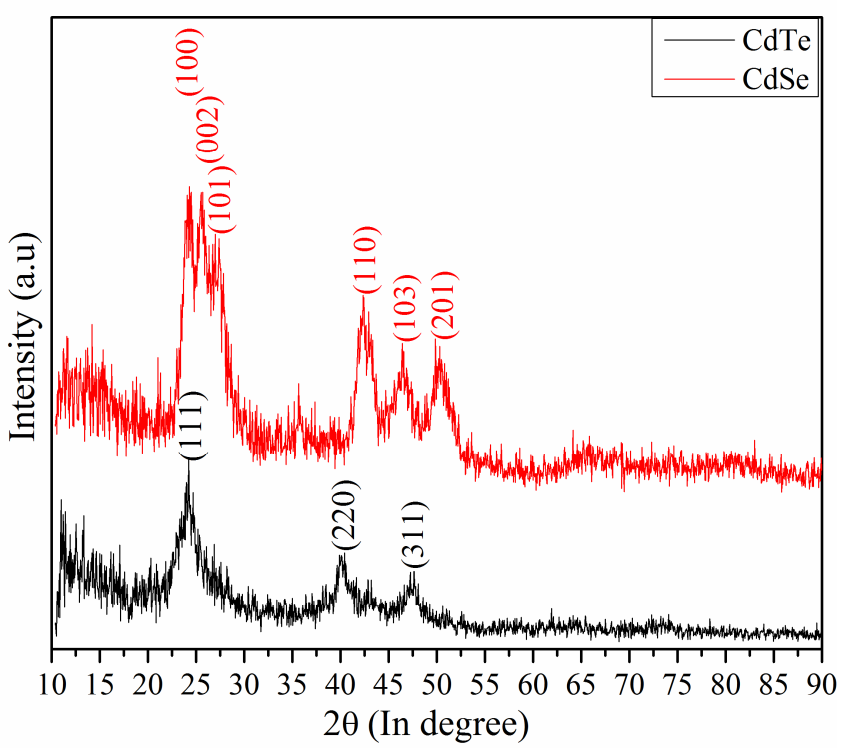

Figure 4.2 XRD pattern of CdTe and CdSe fluorescent quantum dots

Figure 4.2 represents the XRD pattern of both CdTe and CdSe QDs. The broad peaks obtained at 2ɗ values 23.7°, 39.2° and 46.4° corresponds to the (111), (220) and (311) planes of CdTe crystals. The diffractogram of CdSe QDs indicated the presence of (100), (002), (101), (110), (103), and (201) planes at 2ɗ values of 23.8°, 25.3°, 27°, 41.9°, 45.8°, 50.6° respectively. Here, diffraction peaks are indexed to fcc CdTe structure (JCPDS 89-3053) and hexagonal wurtzite phase CdSe crystal structure

(JCPDS 77-2307) [13-15]. The formation of CdS nanocrystal at the surface of CdTe QD was reported when GSH act as a surfactant in the synthesis **[**16, 17]. The probability of formation of CdS nanocrystals at the surface of CdSe is also not neglected when GSH is taken as a surfactant in CdSe QD synthesis**.** This is support by the observed CdS peak after deconvolution of XRD pattern (shown in **figure 4.1A** of **appendix – B)**. The XRD patterns affirm good crystallinity with broad peaks due to the fine dimension of CdTe and CdSe QDs.

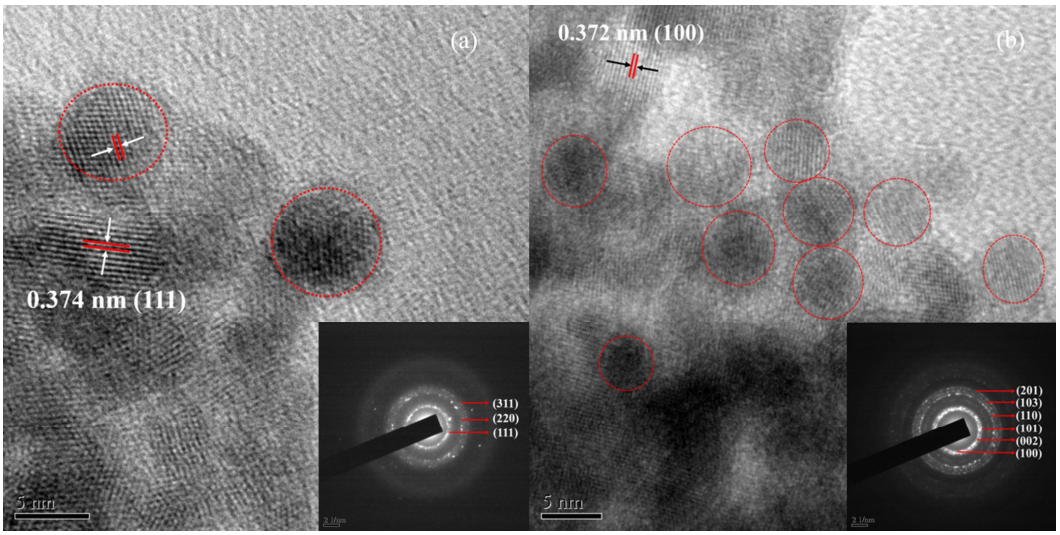

Figure 4.3 HRTEM images of (a) CdTe and (b) CdSe QDs. The insets reveal the respective SAED patterns of QD systems

The morphology of the GSH capped CdTe and CdSe QDs were characterized with high-resolution transmission electron microscopy (HRTEM). **Figure 4.3 (a)** represents the HRTEM micrograph of CdTe QD. The distinct lattice fringe of (111) planes of CdTe is clearly depicted in the micrograph which corresponds to the interplanar d-spacing of 0.374 nm. The inset of **figure 4.3 (a)** shows the SAED pattern analysis of CdTe QD. The presence of (111), (220) and (311) planes corresponds to the primitive fcc phase of CdTe nanocrystal. From the microscopic analysis, it reveals that CdTe QDs have spherical morphology, good crystallinity and an average diameter of ~5 nm with a narrow size distribution.

The HRTEM micrograph of CdSe QD shown in **figure 4.3 (b)** indicates spherical morphology of the QDs. The analysis reveals interplanar spacing of 0.372 nm

corresponding to (100) plane of CdSe crystal. The SAED pattern analysis (inset of **figure 4.3 (b)**) reveals the presence of (100), (002), (101), (110), (103) and (201) planes of hexagonal wurtzite phase of CdSe nanocrystal [18]. From the microscopic analysis, it depicts that CdSe QDs have spherical morphology, good crystallinity and an average diameter of ~5 nm with a narrow size distribution. It is evident that the SAED pattern analyses are in good agreement with the analysis of XRD pattern in both CdTe and CdSe QDs.

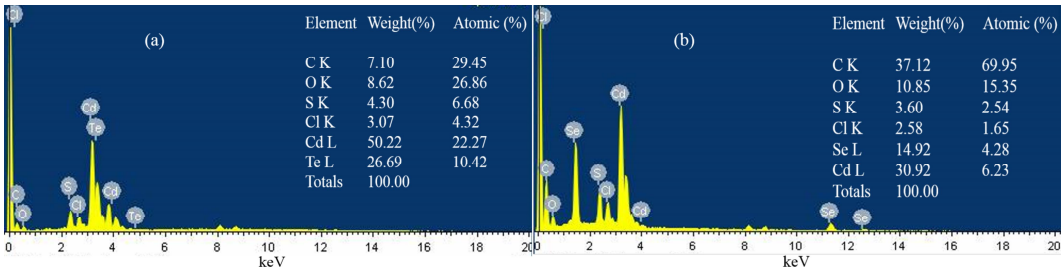

Figure 4.4 EDX spectra of GSH capped (a) CdTe and (b) CdSe QDs. The quantitative data of elements is indicated in each spectrum

EDX was used in the present studies in order to confirm the various elements present in the glutathione capped CdTe and CdSe QDs. **Figure 4.4** displays EDX spectra which confirms presence of signature energy peaks of elements of GSH capped CdTe and CdSe QD systems - C ($K_{\breve{U}}$ line, 0.2 keV), O ($K_{\breve{U}}$ line, 0.5 keV), S ($K_{\breve{U}}$ line, 2.3 keV), Cd ($L_{\breve{U}}$ line, 3.1 keV). The main energy peak of Te ($L\breve{U}$ line, 3.7 keV) is present in CdTe QD spectrum while Se peaks ($K_{\breve{U}}$ line, 11.2 keV; $L_{\breve{U}}$ line, 1.3 keV) is evident in CdSe QD spectrum. The quantitative data (the average value of five different scan) of both the CdTe and CdSe QDs confirms that the atomic ratio of Cd:X (X= Te/Se) is around 2:1. Both the aforesaid QDs systems have some traces of Cl element present as impurities, as seen in the EDX spectra. This is probably coming from the cadmium chloride monohydrate, which was used as Cd source in both the reactions. The XRD and SAED results indicate crystalline fcc-CdTe and wurtzite phase CdSe whereas HRTEMs depict their ultrafine and spherical nature. The EDX pattern analysis reveals the constituent atoms like Cd, Te and Se atoms along with surfactant GSH atoms [19, 20].

The interaction of surface functional groups with QD systems and surface charge provided by GSH molecules were analyzed by using FTIR spectroscopy and zeta

potential respectively. Thermogravimetric (TG) analysis was performed by the thermal analyzer in N_2 atmosphere at the temperature range of 25-600 °C with a heating rate of 10 °C per min.

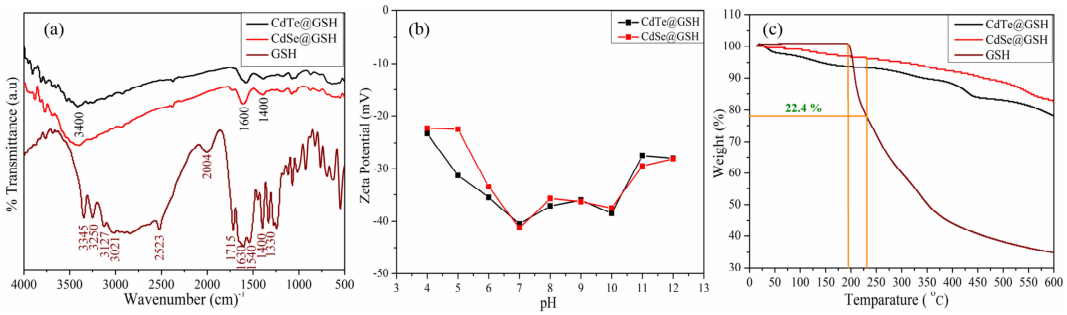

Figure 4.5 Surface characterization of GSH capped CdTe and CdSe QDs. (a) Comparative FTIR spectra of pure GSH, and GSH capped CdTe and CdSe QDs (b) zeta potential curve of both the QD systems (c) A comparative TG analysis of pure GSH, and GSH capped CdTe and CdSe QDs

The comparative FTIR spectra of pure GSH powder and GSH capped CdTe and CdSe QDs are presented in **figure 4.5 (a).** Both QD systems have similar characteristic peaks in FTIR spectra. The L-glutathione (GSH) is a tripeptide molecule made up of one molecule each of L-glutamic acid, L-cysteine and glycine amino acid (ɔ-glu-cys-gly). GSH molecule is rich in functional groups containing two peptides or amide (-CONH-), two -COOH and one -NH_2 group. The FTIR spectrum of pure GSH molecules (**figure 4.5 (a)**) shows two strong bands at 3345 and 3250 cm^{-1} which are assigned to the N-H stretching vibration from the NH_2 molecules present in the glutamic acid residue. In both GSH capped QDs systems, N-H stretching vibrational peak merged into a broad peak which is centered at around 3400 cm^{-1}. The bands present at 3127 and 3021 cm^{-1} in pure GSH molecule is ascribed to N-H stretching vibration of NH_3^+. A strong band at 2523 cm^{-1}, attributed to the -SH stretching vibrations, is present in pure GSH molecules [21, 22]. The absence of S-H peaks in both GSH capped QDs (CdTe and CdSe) indicates the deprotonation of the thiol group and coordination of the thiol group to QD surface. The combined bands of asymmetric NH_3^+ bending vibration and hindered NH_3^+ rotation at 2004 cm^{-1} is present in free GSH molecules. This peak disappeared in case of both the GSH capped QDs (CdTe and CdSe) indicating that the amino group is also

coordinated to surface of QD systems under alkali condition due to the deprotonation of amino group at reaction pH 10. The carboxylic C=O stretching vibration of -COOH group from glycine residue is appearing at 1715 cm^{-1} in pure GSH molecule which shifted to lower frequencies for QD systems around 1600 cm^{-1} possibly due to the deprotonation of -COOH group in the alkaline condition. The characteristic C=O stretching (amide I) and N-H bending vibration (amide II) of the amide bond is appearing at 1630 cm^{-1} and 1540 cm^{-1} in pure GSH molecules [21]. It is noted that the amide I and II vibrational peaks are shifted to lower frequencies i.e. 1600 and 1400 cm^{-1} in both QD systems. The CH_2 bending vibration appears in the range of 1400 cm^{-1} and the band at 1330 cm^{-1} is attributed to the C-N stretching vibration in pure GSH molecule [22]. From aforementioned discussion, it is concluded that in both GSH capped QD systems, the peak appeared at 1600 cm^{-1} has merging of two peaks, C=O stretching vibration of -COOH and amide I group, while the peak appeared at 1400 cm^{-1} also contain merged peaks - one for amide II vibrational and another for CH_2 bending vibration. In both the QD systems, the disappearance of the -SH stretching vibrational peak, the almost disappearance of the N-H and the weakening of the amide bond clearly indicates that GSH have been attached to the surface of QDs through -SH and -NHR groups [23].

The zeta potential, ɛ, is an indicator of particles surface charge and also enables to estimate the stability of the system in the solution. When the ɛ value increases, the repulsion between particles also increases. **Figure 4.5 (b)** indicates characteristic ɛ value of GSH capped CdTe and CdSe QD systems in water. The synthesis of CdTe and CdSe were carried out in alkaline (pH 10) condition. Both the QDs systems exhibit similar surface potential in the zeta potential studies. It is well known that, at lower pH value (pH<3) the GSH molecules develop positive charge whereas for the pH range from 4 to 12 it is mostly dominated by negative charge [24, 25]. Likewise in CdTe and CdSe QD systems, the surface charge ɛ shows a negative potential value in the pH range of 4-12. From the zeta potential analysis, high stability of the QDs can be proposed between pH values 6 to 10. It is because of the fact that the surface potential is maximum i.e. around 38±3 mV at this pH range.

Thermogravimetric (TG) analysis of pure GSH molecules along with GSH capped CdTe and CdSe QD systems are shown in **figure 4.5 (c)**. It is observed that the pure

GSH molecules are stable up to 197 ℃. Both the aforesaid QD systems have the same pattern of degradation as observed from TG analysis curves. The two mass losses at ~ 197 ℃ and 350 ℃ of pure GSH molecules are evolving from the pyrolysis of the oxygenated functional groups and NHS moieties of GSH molecule respectively. Both QD systems lose mass up to 197 ℃, which can be attributed to evaporation of physically adsorbed water molecules [26]. In both QD systems, the slight mass losses at around 400 ℃ and 500 ℃ can be attributed to the degradation of Cd-S or Cd-N bond between the surface of QDs and GSH molecules. The synthesis reaction temperature for the development of both the QD systems was around 230 ℃. The pure GSH molecules lose almost 22 % of their mass while both the QD systems lose almost 1 % of their mass within the temperature range of 197 ℃ to 230 ℃. Thus, the binding of GSH on QDs systems can be inferred. It also indicates that the purification process completely removes free GSH molecules from the QD samples.

Quantum dots absorb photons of light and then re-emit longer-wavelength photons nearly instantaneously. The representative UV-vis absorption and PL spectra of CdTe and CdSe QDs in water are shown in **figure 4.6 (a)**. Both QD systems donôt exhibit a well-deýned absorption feature (peak). It may be due to less concentration of QD systems in aqueous solution while the CdSe reveals a peak ~ 250 nm which is associated with the solvated thiolate anion of GSH molecules [27].

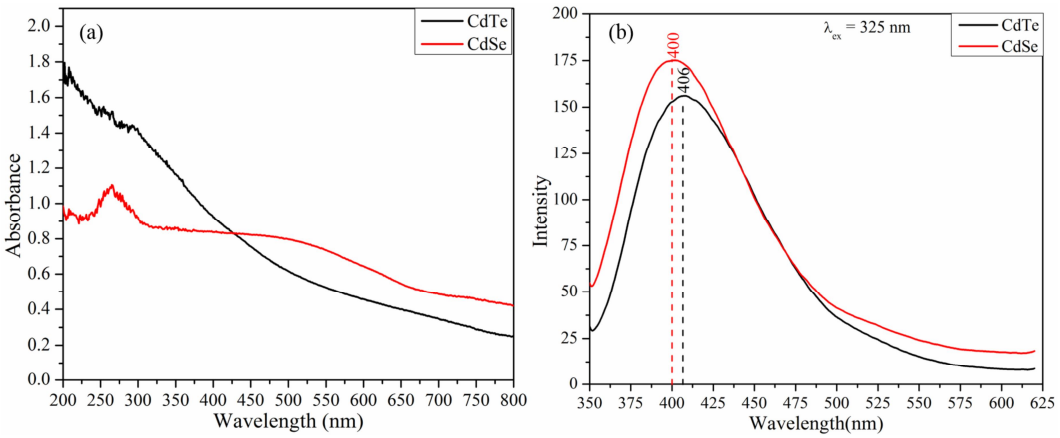

Figure 4.6 (a) UV-vis absorbance and (b) PL spectra of CdTe and CdSe QD systems in water. PL spectra obtained with 325 nm excitation

The CdTe and CdSe fluorescent QDs were excited at different wavelengths between 300-550 nm while the luminescence peak appears only between the wavelengths 300-350 nm. The luminescence intensity changes a bit with excitation wavelength while the emission peak position and shape of pattern almost remain the same. The maximum intensity of PL for both the QD systems is observed at an excitation wavelength of 325 nm. **Figure 4.6 (b)** exhibits the PL emission peak of CdTe and CdSe QDs at ~ 406 and 400 nm respectively when it was excited at 325 nm. It is seen that the PL peaks of both QD systems are asymmetrical. Therefore, deconvolution of PL spectra along with time-resolved photoluminescence (TRPL) spectra are presented in **figure 4.7** for both QDs systems. The peak of interest was selected and fitted using Gaussian function with multiple peak fitting option. It was done in Origin software.

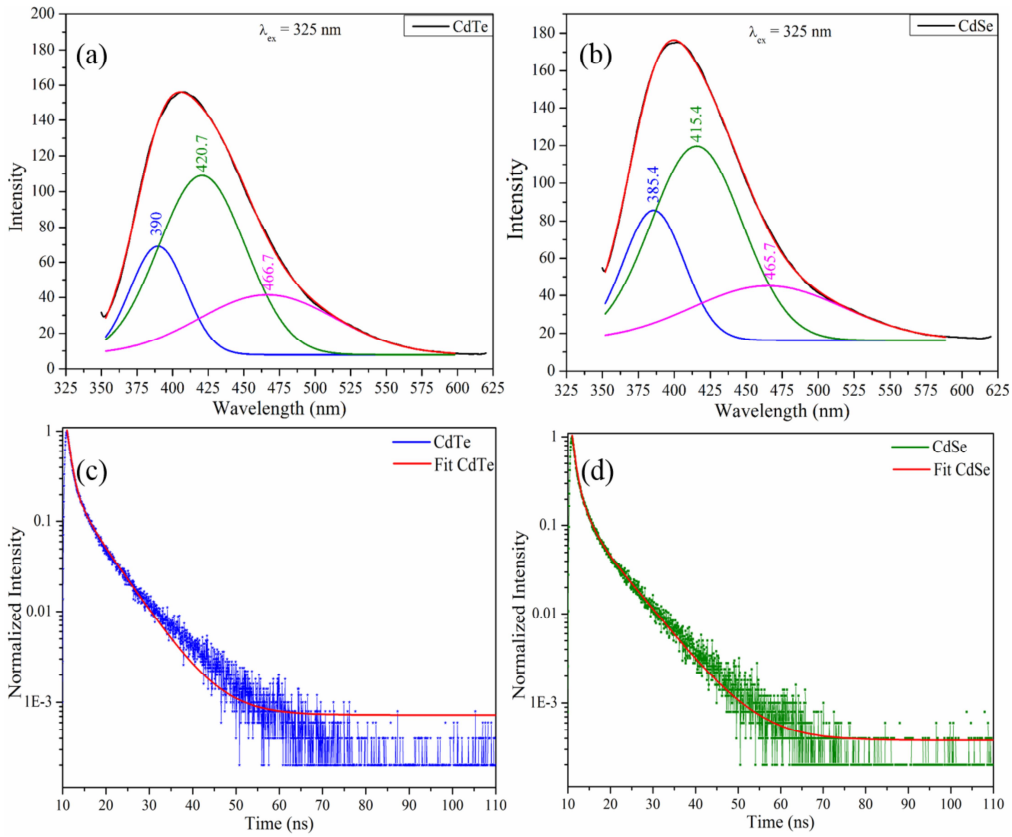

Figure 4.7 Deconvoluted PL (a & b) and TRPL (c & d) spectra of CdTe and CdSe QD systems respectively. The solid line is a single exponential fit to the data.

Gaussian deconvolution of PL spectra of CdTe and CdSe QDs systems shown in **figure 4.7** (a, b) reveals that the spectra consist of three emission peaks. Both the CdTe and

CdSe systems exhibit almost similar emission profiles. To identify the origin of all the emission peaks TRPL analysis was carried out. TRPL spectra shown in **figure 4.7** (c & d) were best fitted with the tri-exponential decay function as given below-

$$I = A_1 \exp\left(-\frac{t}{\tau_1}\right) + A_2 \exp\left(-\frac{t}{\tau_2}\right) + A_3 \exp\left(-\frac{t}{\tau_3}\right)$$

Where, I is the PL intensity, A_1, A_2 and A_3 represent the amplitudes of three decay processes, t-decay time, τ_1, τ_2 and τ_3 represent the three decay lifetimes. Values of lifetime components and their amplitudes (%) for each system are shown in **table 4.1**. The fast lifetime component may be due to the direct band-edge excitonic recombination, while other two longer components can be observed due to the radiative recombination of electrons and holes at localized surface states [28, 29]. Thus, the peaks around 390 nm can be assigned to the band edge type emission while the other two peaks around 420 nm and 460 nm can be assigned to surface state emission. The average lifetime for each TRPL data is calculated using the following equation:-

$$\langle \tau \rangle = \frac{\sum_i A_i \tau_i^2}{\sum_i A_i \tau_i}$$

For both the QD systems, it is observed that the amplitudes of the fastest components are predominant over other two components.The average carrier lifetime is obtained higher for CdTe system while the calculated quantum yield shows higher value for the CdSe system. The higher average lifetime for the CdTe system is resulting from the higher lifetime amplitudes of defect related decays, which signifies that the density of defect states are more in the CdTe system in comparison to the CdSe systems.

Table 4.1 Decay components obtained from TRPL results for both CdTe and CdSe QDs

Systems	**Decay components**							
	τ_1 (ns)	YS (%)*	τ_2 (ns)	YL_1 (%)*	τ_3 (ns)	YL_2 (%)*	$\langle\tau\rangle$ (ns)	(%) QY
CdTe	0.088	95	1.71	4.23	7.20	1.35	3.29	0.98
CdSe	0.0496	97.9	1.72	1.64	7.67	0.47	2.9	1.71

*YS (%) - percentage amplitude of the fast component

*YL (%) - percentage amplitude of the longer component.

These are calculated using the equation $Y_i = \frac{A_i}{\sum_i A_i} \times 100$.

The easiest way to estimate the quantum yield (QY) of QDs is comparing a standard sample with a known quantum yield (QYô). Rhodamine 6G in water was used here as a reference.

The quantum yield of QDs can be calculated by using following equation-

$$QY = QY' \times (I / I') \times (A' / A) \times (\eta / \eta')^2 \times 100$$

where,

I = Integrated area of sample

Iô = Integrated area of Rhodamine

A = Absorption of sample

A` = Absorption of Rhodamine

ɖ = Refractive index of sample

ɖ` = Refractive index of standard

The QY of rhodamine 6G is known to be 95%. The luminescent property is supported by the calculated quantum yield (QY) values as shown in **table 4.1**.

Toxicity Assay- Resazurin Reduction Assay

QDs may have various applications in technology, research, and medicine due to their unique and attractive properties. Hence, a detailed toxicity assessment is important in the case of QDs for their potential in biomedical applications. For quantifying *in vitro* cell viability with CdTe and CdSe QD samples, Resazurin Reduction Assay or Alamar Blue (AB) toxicity assay was performed. AB toxicity assay has been considered superior to other classical assays for cell viability because its reagent is extremely stable, water soluble, non-toxic to the cells and continuous monitoring of cultures is possible with time.

Cell line

For determining the toxicity effect of the as-prepared QDs Murine RAW 264.7 macrophage cell lines were employed.

Chemicals and reagents

Dulbeccoôs modiýed Eagleôs medium (DMEM), Hanks balanced salt solution (HBSS), Fetal bovine serum (FBS), antibiotics (gentamicin, amphotericin B and streptomycin), trypsin, trypan blue and resazurin were procured from Sigma-Aldrich (St. Louis, USA). Milli-Q Type I water was used for experiments.

Cell culture

CO_2 incubator (Innova-CO170; New Brunswick Scientific, USA), phase contrast inverted microscope (Zeiss-AXIO, Carl Zeiss, Germany) with AxioCam ERc 5s camera and Axiovision SE64 Rel 4.9 software (Carl Zeiss, Germany), biosafety cabinet (CBS900, Clean Air system, India), water bath (Equitron, India), refrigerated centrifuge (Sigma 3-30K, Sigma Lab. Gmbh, Germany), cell culture flask and plastic wares (BD Biosciences, USA), liquid handling apparatus (Eppendorf, Germany), microplate reader (SpectraMax Plus-384, Molecular Devices, USA).

Methods

Murine RAW 264.7 macrophage cells were cultured in DMEM supplemented with 10% FBS, 100 µg/ml of penicillin, 100 µg/ml of streptomycin at 37 °C, in an atmosphere of 5 % CO_2 and 90 % relative humidity. The cells were sub-cultured after every 2-3 days at 1:5 split ratios.

The RAW 246.7 toxicity assay was performed as per the reported method [30, 31]. Conþuent murine macrophages were harvested, centrifuged and re-suspended in DMEM supplemented with 10 % FBS and the cell density was adjusted to 10,000 cells/100 µl in the cell suspension. 100 µl of cell suspension containing $1x10^4$ cells was seeded to each well of 96 well plates, excluding ýrst row with the aid of manually handy process. After that, the plate was incubated at 37 °C, in an atmosphere of 5 % CO_2 and 90 % relative humidity for 1 hour. After 1 hour, the test sample volume 0.1 mL, 0.075 mL, 0.05 mL and 0.025 mL (dose dependent concentration) were added to the wells of 96 well plates in triplicate culture. The 96 well plates were then incubated

for 24 hour at 37 °C in an atmosphere of 5 % CO_2 and 90 % relative humidity. The experiment was repeated three times.

Alamar Blue (AB) reagent (resazurin) was added at the end of 24 hours incubation, to 96 well plate having cells growth. Initially, there was no colour change in the wells upon addition of AB reagent. The non-fluorescent blue dye, resazurin (7-hydroxy-10-oxidophenoxazin-10-ium-3-one) is reduced to the fluorescent pink resorufin (dye) and dihydroresorufin by viable, metabolically active cells only. This conversion occurs in the cytosol of viable and metabolically active cells with the help of mitochondrial enzyme activity by accepting electrons from, FADH, NADPH, and NADH etc. The 96 well plate was then incubated for 1-4 hour at 37 °C and reaffirmed for colour change. The absorbance signal is monitored at 540 nm. Absorbance data was collected in SpectraMax Plus 384 microplate reader (Molecular Devices, USA). After calculation of mean and standard deviation (SD = ů) from the repeated experiments, the cell viability was calculated using following formula:-

$$\text{Cell Viability (\%)} = \frac{(\text{mean absorbance value of experimental group})}{(\text{mean absorbance value of control group})} \times 100$$

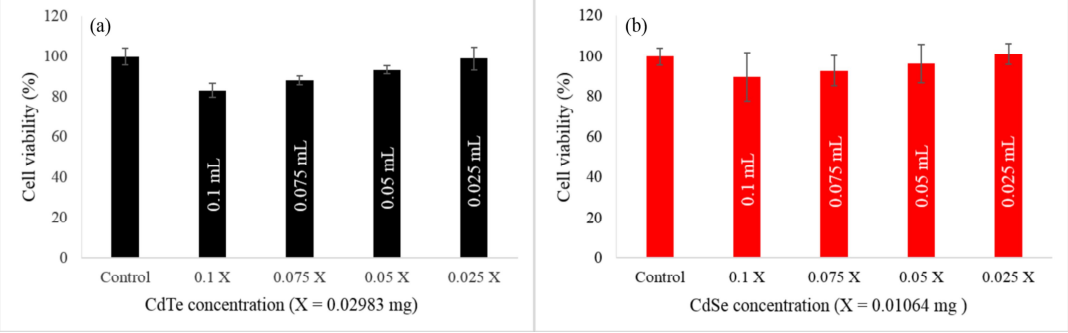

Figure 4.8 Viability of RAW 264.7 macrophage cell line compared to control indicated by AB assay when cell was exposed to GSH capped (a) CdTe and (b) CdSe QDs. The error bar was drawn using SD value.

Figure 4.8 exhibits the viability of RAW 264.7 macrophage cell line with different doses of quantum dots. The concentration of CdTe and CdSe QD stock solutions used in the experiment were 0.02983 and 0.01064 mg/mL respectively. Dose-dependent

concentration of QD systems is put in **table-4.2**. The control contains only media and cells and is devoid of any QD sample. The % cell viability of control is taken as reference for calculation of cell viability with samples [32]. From both the graphs, it is seen that the viability of RAW 264.7 macrophage cell lines is not affected (< 80 %) by CdTe and CdSe QDs even at 0.1 mL (0.000266 mg) concentration. It is also observed that when the dose of CdTe and CdSe was decreased i.e. when the volume of test sample decreases, the viability of the cell increases. At the lowest dose, i.e. in 0.025 mL volume (0.000745 mg; CdTe and 0.000266 mg; CdSe) the viability is close to 100 % in case of both samples.

Table 4.2 Dose dependent concentration of QD systems

Si. no.	Sample	Concentration (Stock)	Volume	Dose dependent concentration
1	CdTe	0.02983 mg / mL	0.1 mL	0.002983 mg
			0.075 mL	0.002237 mg
			0.05 mL	0.001491 mg
			0.025 mL	0.000745 mg
2	CdSe	0.01064 mg / mL	0.1 mL	0.001064 mg
			0.075 mL	0.000798 mg
			0.05 mL	0.000532 mg
			0.025 mL	0.000266 mg

To investigate the imaging capability of GSH capped CdTe and CdSe QD, cells were taken out from 96 well plates after toxicity assay which contained 0.1 mL volume of QD systems. These cells contain fluorescent pink resorufin and produced a fluorescent signal when it is excited at wavelength 530-560 nm. In the imaging process, the samples were excited at UV, blue and green lights and their wavelengths (ƛ) were corresponding to 360, 450 and 530 nm respectively. The fluorescence image obtained using UV and

blue excitation was exclusively due to quantum dot fluorescence whereas the green light excited fluorescence image have additional fluorescent contribution due to dye. This finding is supported by observed mild fluorescence in a control cell when it is excited at 530 nm. The fluorescence images of control cell are placed in **figure 4.1B** of **appendix - B**. The fluorescence images of both the GSH capped QDs in RAW macrophage cells were taken on Leica trinocular inverted research microscope (Leica DMI 6000 B) with a magnification of 63X using an oil-immersion objective lens [33, 34]. **Figure 4.9** and **4.10** reveal images (bright field and fluorescence) of GSH capped CdTe and CdSe QDs respectively. The bright field images **figure 4.9 (a)** and **4.10 (a)** reveal no signature of morphological damage to the cells upon treating with CdTe and CdSe QDs respectively.

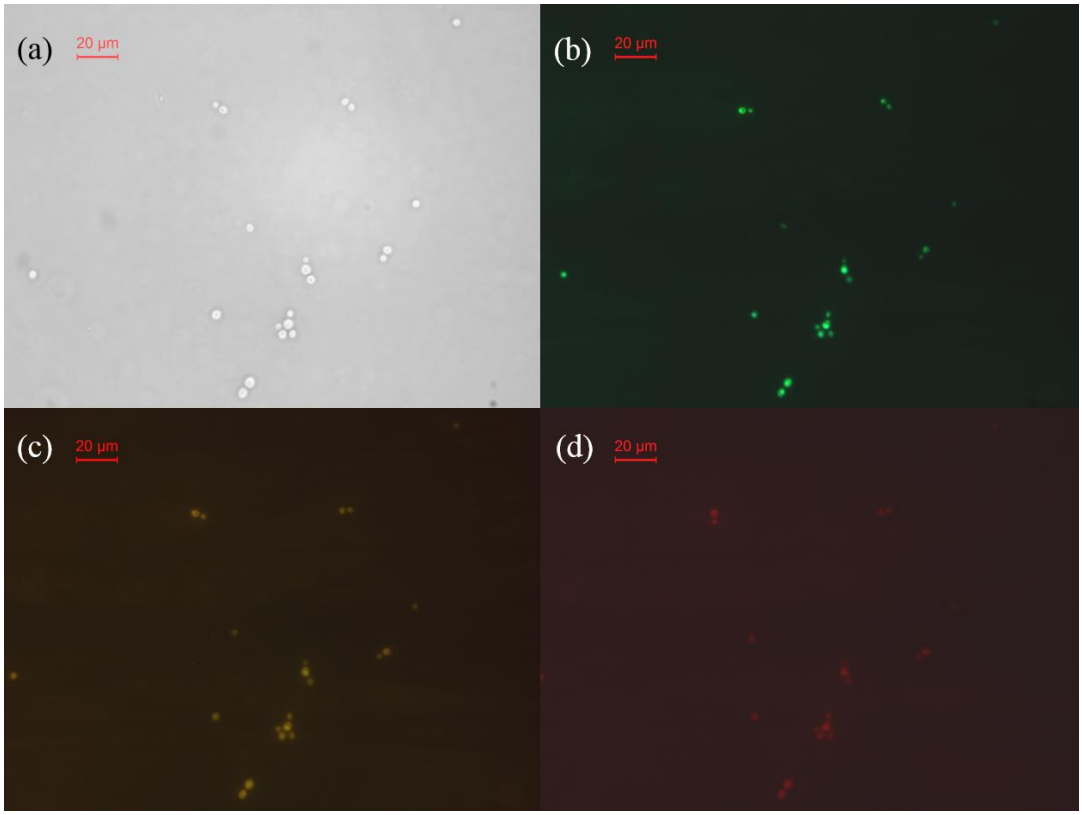

Figure 4.9 *In vitro* bright field and fluorescence images of GSH capped CdTe QDs in RAW 264.7 macrophage cells. Images were taken in inverted research microscope under (a) bright field, (b) UV, (c) blue and (d) green light.

Fluorescence micrographs were taken for realizing the fluorescence efficiency of QDs system. Fluorescence images corroborates with the results of toxicity assay i.e. good

biocompatibility. F**igure 4.9 (b)** and **4.10 (b)** depict bright green fluorescence when the UV light passed through the filter. Simultaneously, the **figure 4.9 (c) & (d)** reveals a light yellow and red fluorescence produced when blue and green light passed through the filter. Whereas **figure 4.10 (c) & (d)** reveals red fluorescence, when blue and green light are allowed to pass through. But, the intensities of fluorescence image decreases under blue and green light as compared to UV light in both cases.

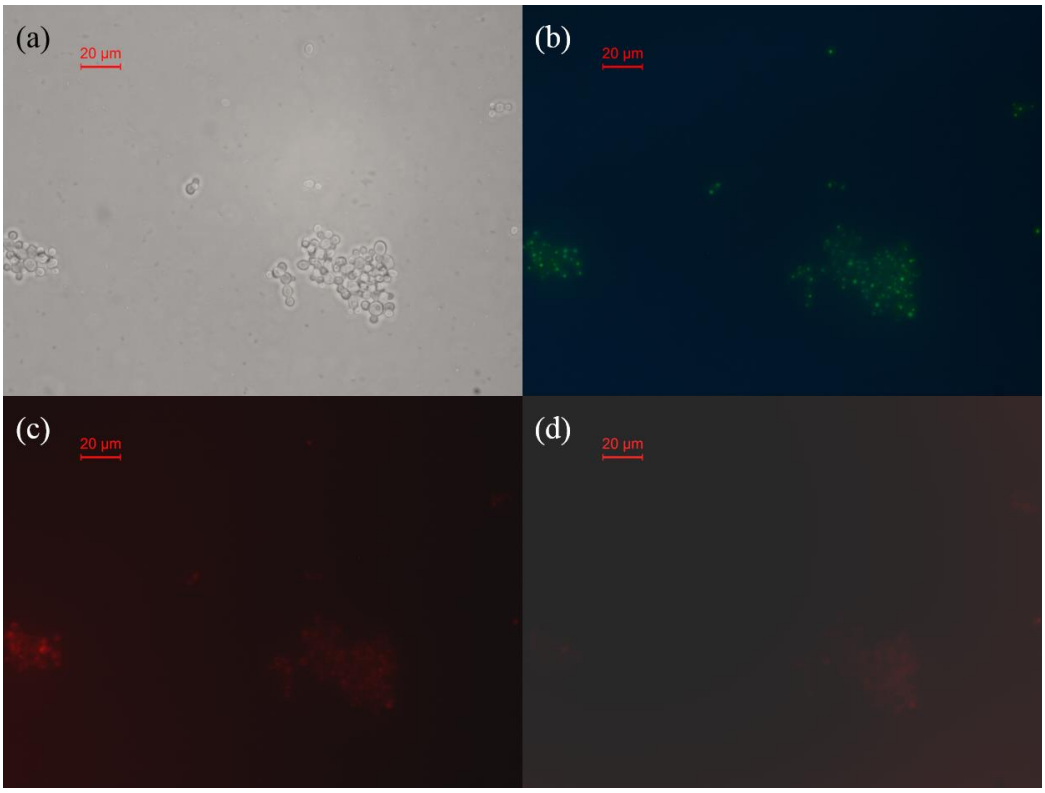

Figure 4.10 *In vitro* bright field and fluorescence images of GSH capped CdSe QDs in RAW 264.7 macrophage cells. Images were taken in inverted research microscope under (a) bright field, (b) UV, (c) blue and (d) green light.

It is worthwhile to mention here that the use of organic fluorophores for imaging applications is subject to certain limitations. Organic fluorophores are restricted by their narrow excitation and emission spectra whereas QDs can be excited by any wavelength from UV to red for obtaining the different colour of fluorescence images. The GSH capped CdTe and CdSe QDs shows good biocompatibility and are capable of imaging of cell without interference with the growth or differentiation of the cells. Hence, the

present QD systems can be used as a promising alternative to organic dyes for fluorescence-based biomedical applications.

Section-B

4.5 Synthesis of CdS fluorescent quantum dots

The GSH capped CdS fluorescent quantum dots (QDs) were developed using a facile one-pot polyol process. The reaction was carried out in 100 mL three-necked flask with a reflux condenser in an open atmosphere. In a typical reaction process, 2.5 mmol cadmium chloride monohydrate was dissolved in 5 ml of ethylene glycol and was added to 20 mL of ethylene glycol in the three-necked flask (**refer figure 4.11 (a)**). A schematic diagram representing synthesis steps and changing colour conditions of the reaction liquid in the synthesis of CdS QDs is shown in **figure 4.11**.

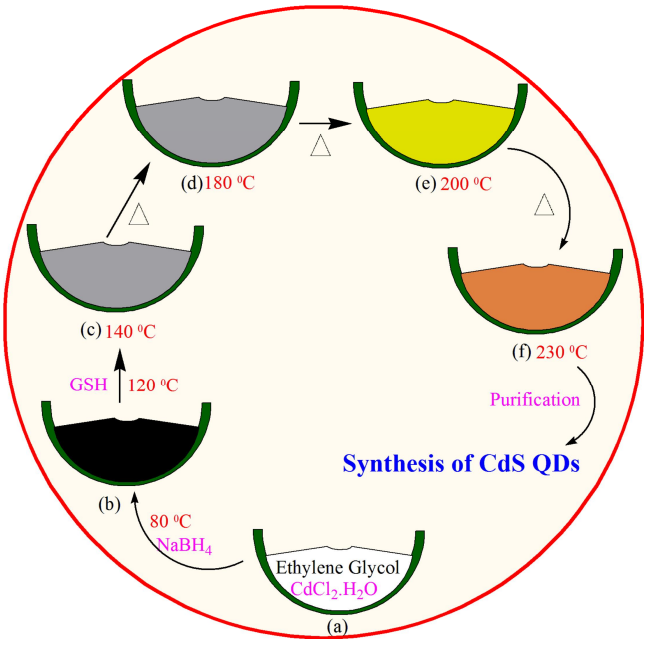

Figure 4.11 Schematic diagram represents steps involved in synthesis of GSH capped CdS fluorescent QDs

The temperature of the reaction vessel was slowly increased. When the temperature increased to 80 °C, 4 mmol $NaBH_4$ was added to the reaction vessel. After addition of

reducing agent, the colour of reaction liquid turns into black, might be due to the reduction of Cd (**refer figure 4.11 (b)**). At 120 ℃, 0.5 mmol glutathione in 5 mL ethylene glycol was added dropwise to the reaction mixture. After addition of GSH, the reaction medium changed its colour from grey to black. The molar ratio of Cd and GSH was maintained to 5:1. Here, GSH acted as a sulfur source as well as the capping agent. After attending 140 ℃, maintain this temperature for 15 minutes then heating up to 180 ℃ at constant rate 1 ℃/min (**refer figure 4.11 (c & d)**). The onward reaction temperature was then further increased at the rate of 1 ℃/min to 230 ℃. At 200 ℃, the reaction medium further changed its colour to light yellow finally turning into golden brown colour at 230 ℃ (**refer figure 4.11 (d & e)**). When the reaction temperature reached to 230 ℃, the heating was stopped and the reaction vessel was allowed to cool down.

The precipitate was separated from the reaction mixture by centrifugation and subsequently washed three times using hexane, isopropyl alcohol and methanol to remove the residual surfactants. The purified mass obtained was yellow in colour which was used for further characterization.

4.6 Characterization

The synthesized CdS QDs was characterized using several techniques for in-depth understanding of properties.

4.6.1 Results and discussion

The crystallographic structure of CdS QDs were characterized by X-ray diffraction (XRD) using a Rigaku diffractometer with Cu Kŭ1 radiation (ə= 1.5406 Å). As seen in **Figure 4.12,** the diffractogram shows the presence of broad peaks at 2ɗ ~ 24.8°, 26.5°, 28.1°, 36.6°, 43.6°, 47.8° and 51.8° corresponding to the (100), (002), (101), (102), (110), (103) and (112) planes of hexagonal wurtzite phase CdS (JCPDS 89-2944) [35, 36]. It is seen that the lattice constant values, a = 0.4132 and c = 0.6715 nm, are consistent with the standard values for bulk CdS. However, the formation of CdO lattice is not evident in the XRD pattern of CdS QDs.

Detailed structural, morphological and compositional studies of the CdS QDs were carried out using various analytical techniques such as HRTEM, SAED and EDX. **Figure 4.13 (a)** depict HRTEM micrograph of CdS fluorescent QDs. It is evident from the micrograph that the morphology of the QDs varies from near spherical to a spherical shape.

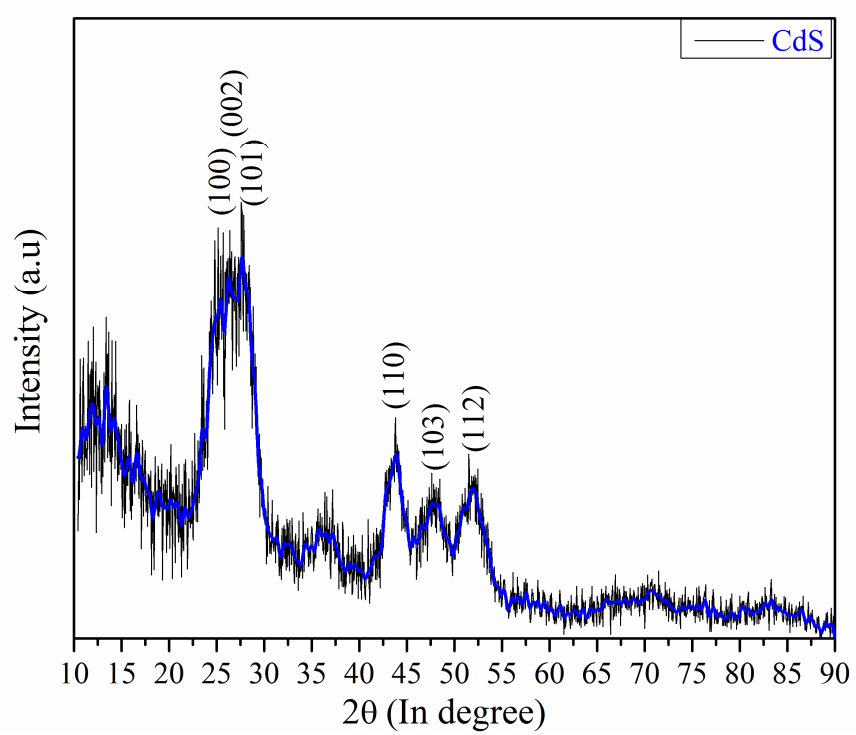

Figure 4.12 XRD pattern of fluorescent CdS QDs

In this system, the interplanar distance (d) is obtained as 0.35 nm which is assigned to the (100) plane of CdS nanocrystal. The SAED pattern analysis (**figure 4.13 (b)**) reveals presence of (100), (002), (101), (110), (103) and (112) planes corresponding to hexagonal wurtzite phase of CdS crystals. The EDX spectrum of CdS shown in **figure 4.13 (c)**, indicates the presence of the main signature peak of the elements present in the sample - C ($K_{\breve{U}}$ line, 0.2 keV), O ($K_{\breve{U}}$ line, 0.5 keV), S ($K_{\breve{U}}$ line, 2.3 keV), and Cd ($L_{\breve{U}}$ line, 3.1 keV). The inset of figure 4.13 (c) reveals the atomic weight % of the elements obtained from the average value of five different scan. The trace amount presence of Cl, indicated in the EDX spectra, is probably due to the cadmium chloride monohydrate which was used as Cd source in the reaction.

The interaction between the surface coating molecule GSH and the CdS QDs was studied by FTIR spectroscopy, zeta potential and thermogravimetric analysis. A detailed FTIR analysis of pure GSH compound is discussed in previous section-A **(figure 4.5 (a)).**

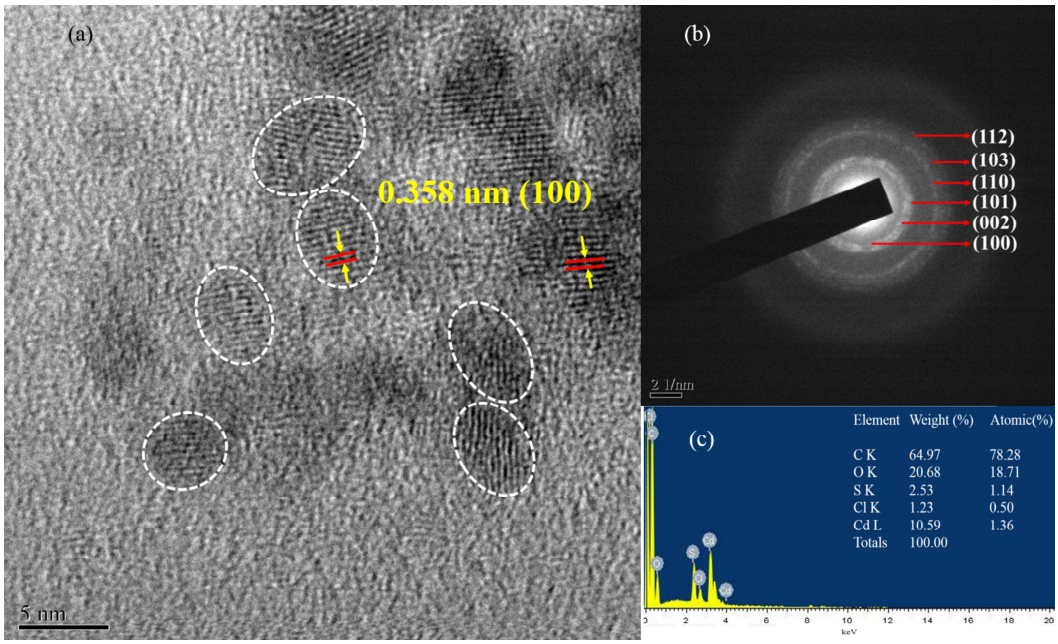

Figure 4.13 Microstructural and compositional characterization of CdS QDs (a) HRTEM image, (b) SAED pattern and (c) EDX with weight and atomic % of element

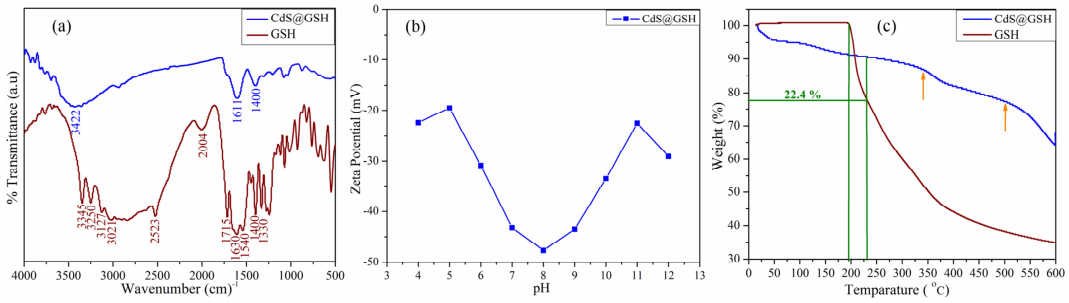

Figure 4.14 Surface characterization of GSH capped CdS fluorescent QDs. (a) comparative FTIR spectra of pure GSH and CdS QDs (b) zeta potential of CdS QDs and (c) A comparative TG spectra of pure GSH and CdS QDs

F**igure 4.14 (a)** represents the comparative FTIR spectra of pure GSH with GSH capped CdS QDs. Briefly, in case of pure GSH, a strong band at 2523 cm^{-1} is observed due to the -SH stretching vibrations. The -SH band is absent in the FTIR spectrum of CdS

QDs. It is due to the deprotonation of the thiol group and coordination of the thiol group to the surface of CdS QDs [37]. The combined bands of asymmetric NH_3^+ bending vibration and hindered NH_3^+ rotation at 2004 cm^{-1} seen in pure GSH disappeared in GSH capped CdS. Hence, it can be attributed that the amino group is in coordination to the surface of QDs which is due to the deprotonation of an amino group. The band at 3422 cm^{-1} in the GSH capped CdS QDs is due the stretching vibration of ï OH group. The characteristic C=O stretching (amide I) and N-H bending vibration (amide II) of amide bond are expressed at 1630 and 1540 cm^{-1} in pure GSH molecules. However, amide I and II vibrational peaks are shifted to the lower frequency at 1600 and 1400 cm^{-1} in the case of the GSH capped CdS QDs system. In both the QD systems, the disappearance of the -SH stretching vibrational peak, the slurring of the N-H band and the weakening of the amide band clearly indicates that GSH has been bound to the surface of the QDs through the -SH and -NHR groups [21-23].

Figure 4.14 (b) indicates the zeta potential (ɛ) value of GSH capped CdS QDs system in water. Between pH of 4 to 12, the GSH capped CdS QDs displays a negative potential while, at physiological pH, the potential value rises up to -45 mV [24, 25]. The Zeta potential studies reveal that these QD systems are in stable solution in water. The thermogravimetric (TG) analysis study of pure GSH molecules and CdS QDs coated with glutathione is shown in **figure 4.14 (c)**. There is a measurable difference observed in weight loss between TG curve of pure GSH molecules and GSH capped CdS QDs. It is seen that the stability of GSH molecules increased after attachment with the QD system. The TG study reveals ~ 10% weight loss from room temperature to ~197 °C in GSH capped CdS QDs corresponding to the removal of water molecules. There is ~ 10 % mass loss between 350 to 500 °C in GSH capped CdS QDs whereas this difference is ~ 13 % in free GSH molecules. The mass loss at ~ 350 and 500 °C can be attributed to the loss of the labile oxygen-containing functional groups of GSH and degradation of Cd-S bond present at the surface of GSH capped CdS QDs [26]. The comparative mass loss between RT to 600 °C is ~ 65.2 and 35.8 % in free GSH molecules and GSH capped CdS QDs respectively. There is big mass loss difference between free GSH molecules and GSH capped QDs systems. This can be due to binding of GSH molecule on the CdS particles and absence of free GSH molecules in the sample after purification.

Figure 4.15 (a) and (b) indicates UV absorption curve and corresponding photoluminescence (PL) spectrum of CdS QDs recorded at room temperature. The UV absorption peak seen at ~ 432 nm is characteristics peak for CdS QDs whereas the bulk CdS reveal absorbance at ~ 516 nm [38]. The blue shift of the absorption edge is due to the decrease of the crystallite sizes in CdS QDs which is also known as quantum confinement effect. Fluorescence spectra of the spherical CdS QDs were measured with varying excitation wavelengths from 250 to 440 nm. The fluorescence intensity changes slightly with the excitation wavelength while the fluorescence peak position and peak shape remain the same.

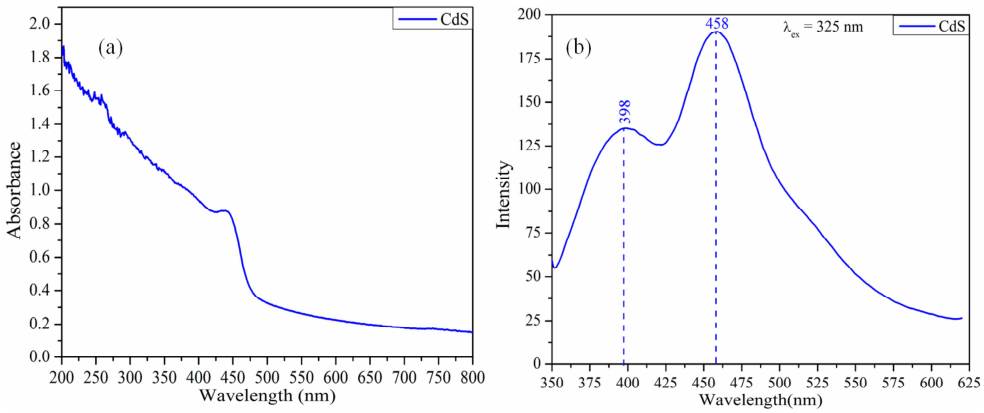

Figure 4.15 (a) UV-vis absorbance and (b) PL spectrum of GSH capped CdS QDs system in aqueous suspension. The PL spectrum was taken at excitation 325 nm

This reveals that the emission spectrum is almost independent of the excitation wavelength used. It is observed that the maximum PL intensity is found at λ_{ex} = 325 nm. It is known that the band edge emission of CdS QDs is observed around 400-440 nm. Here, the fluorescence spectrum of the CdS QDs shows a band edge emission at ~ 398 nm and a broad trap state emission centered around 458 nm.

For understanding different types of emissions, the asymmetric PL spectrum of CdS QDs system was deconvoluted with Gaussian function as shown in the **figure 4.16 (a).** Fitting shows the presence of three peaks centered on 393, 456 and 485 nm with the fitness of the curve R^2 = 0.99. The CdS QDs also express three peaks at around 393, 456 and 485 nm with the fitness of the curve R^2 = 0.99. Initial peak ranging 393 nm arises due to the band edge emission whereas the other two peaks around 456 & 485 nm are

due to the defect states. The origin of all emission peaks and their evolution during CdS QDs was corroborated by analyzing the TRPL (time resolved photoluminescence) data **figure 4.16 (b)**. TRPL spectrum was best fitted with the tri-exponential decay function as given below-

$$I = A_1 \exp\left(-\frac{t}{\tau_1}\right) + A_2 \exp\left(-\frac{t}{\tau_2}\right) + A_3 \exp\left(-\frac{t}{\tau_3}\right)$$

Where, I is the PL intensity, A_1, A_2 and A_3 represent the amplitudes of three decay processes, t-decay time, τ_1, τ_2 and τ_3 represent the three decay lifetimes.

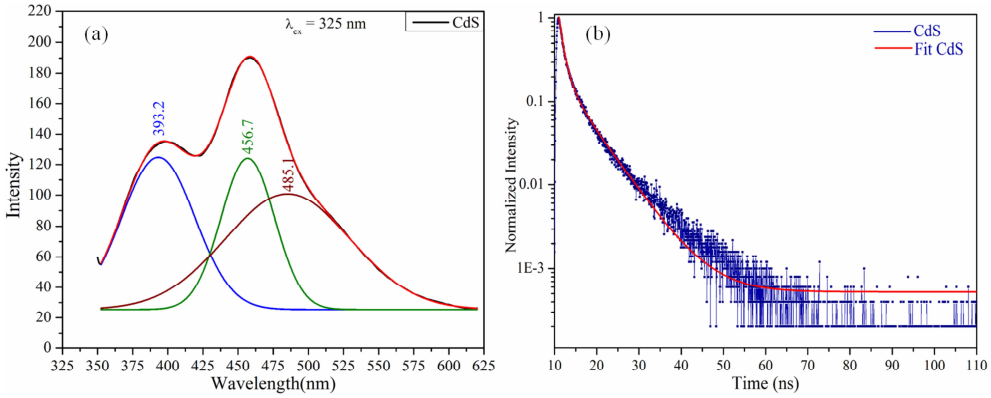

Figure 4.16 (a) Deconvolution of the PL spectrum (λ_{ex} = 325 nm) and (b) TRPL spectrum of CdS QDs in aqueous suspension

The value of lifetime components and their amplitudes (%) for each system are shown in **table 4.3** [28, 29]. The fast lifetime component might be due to the direct band-edge excitonic recombination while other longer components can be observed due to the radiative recombination of electrons and holes at localized surface states.

Table 4.3 Decay components obtained from TRPL results for CdS quantum dots

QDs System	Decay components						
	τ_1 (ns)	YS (%)*	τ_2 (ns)	YL_1 (%)*	τ_3 (ns)	YL_2 (%)*	$\langle\tau\rangle$ (ns)
CdS	0.764	72.8	2.859	21.77	8.70	5.34	3.8

The average lifetime for each TRPL is calculated using the following equation-

$$\langle \tau \rangle = \frac{\sum_i A_i \tau_i^2}{\sum_i A_i \tau_i}$$

The increase in an average lifetime signifies the radiative emission stability of the systems. The luminescent property is supported by the calculated quantum yield (QY) value of 1.67 % for CdS QDs [13].

For quantifying *in vitro* cell viability with the as-prepared QD system, Resazurin Reduction Assay or Alamar Blue (AB) toxicity assay was performed [30, 31]. The detailed procedure is explained in **section – A** of this chapter. Briefly, Murine RAW 264.7 macrophage cell line was used for performing the toxicity assay.

100 µl of cell suspension containing $1x10^4$ cells was seeded into each well of 96 well plates, excluding the ýrst row. After that, the plate was incubated at 37 °C, in an atmosphere of 5 % CO_2 and 90 % relative humidity for 1 hour (h). The concentration of CdS stock solution was 0.05115 mg/mL. Dose-dependent concentration of CdS QD systems is put in **table-4.4**. After 1 hour, test sample volume of 0.1 mL (0.005115 mg), 0.075 mL (0.003836 mg), 0.05 mL (0.002557 mg) and 0.025 mL (0.001278 mg) (volume dependent concentration) were added to the wells of 96 well plates in triplicate culture. The 96 well plates were then incubated for 24 hour at 37 °C in an atmosphere of 5 % CO_2 and 90 % relative humidity. The experiment was repeated three times.

Table 4.4 Dose dependent concentration of CdS QD system

Si. no.	Sample	Concentration (Stock)	Volume	Dose dependent concentration
1	CdS	0.05515 mg / mL	0.1 mL	0.005115 mg
			0.075 mL	0.003836 mg
			0.05 mL	0.002557 mg
			0.025 mL	0.001278 mg

Alamar Blue (AB) reagent (resazurin) was added at the end of the 24 hours incubation to the 96 well plate having cell growth. The 96 well plates was then incubated for 1-4 hour at 37 °C and reaffirmed for colour change. The absorbance signal is monitored at 540 nm. Absorbance data was collected in SpectraMax Plus 384 microplate reader (Molecular Devices, USA) reader at 540 nm. After calculation of mean and standard deviation (SD = ů) from the repeated experiments. The cell viability was calculated using following formula:-

$$\text{Cell Viability (\%)} = \frac{(\text{mean absorbance value of experimental group})}{(\text{mean absorbance value of control group})} \times 100$$

Figure 4.17 exhibits the viability of RAW 264.7 macrophage cell line with different dosages of quantum dots. The control was devoid of the test sample and it contained media and cells only.

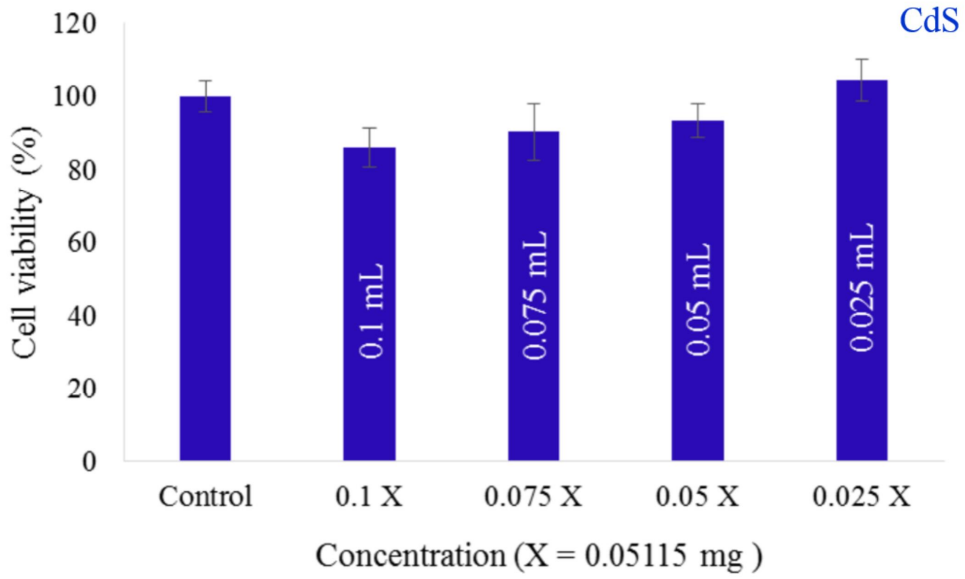

Figure 4.17 Viability of RAW 264.7 macrophage cell line compared to control indicated by AB assay when the cell was exposed to (a) GSH capped CdS QDs. The error bar was drawn using SD value

The cell viability of the control is taken as reference for calculation of % cell viability with different dose of CdS QDs [32]. The graph exhibits that the RAW 264.7

macrophage cell lines were not affected (< 80 %) by CdS QDs even at 0.1 mL concentration. It is also observed that when the mass of CdS is decreased i.e. the volume of test sample decreased, the viability of the cell increases. At lowest mass, i.e. in 0.025 mL volume, the viability is close to 100 % in case of samples.

The fluorescence functionality of GSH capped CdS QDs in RAW 264.7 macrophage cells was studied using Leica trinocular inverted research microscope (Leica DMI 6000 B) having a 63X oil-immersion objective lens. For *in vitro* imaging, cells were taken out from 96 well plates after toxicity assay which contained 0.1 mL volume of CdS solution. **Figure 4.18** depicts bright field and fluorescence images of GSH capped CdS QDs [33, 34]. These cells contain fluorescent pink resorufin and hence showed fluorescence at an excitation wavelength of 530-560 nm **(figure 4.1B** of **appendix B**). In the imaging process, the samples were excited at UV, blue and green lights and their wavelengths (ƛ) correspond to 360, 450 and 530 nm respectively.

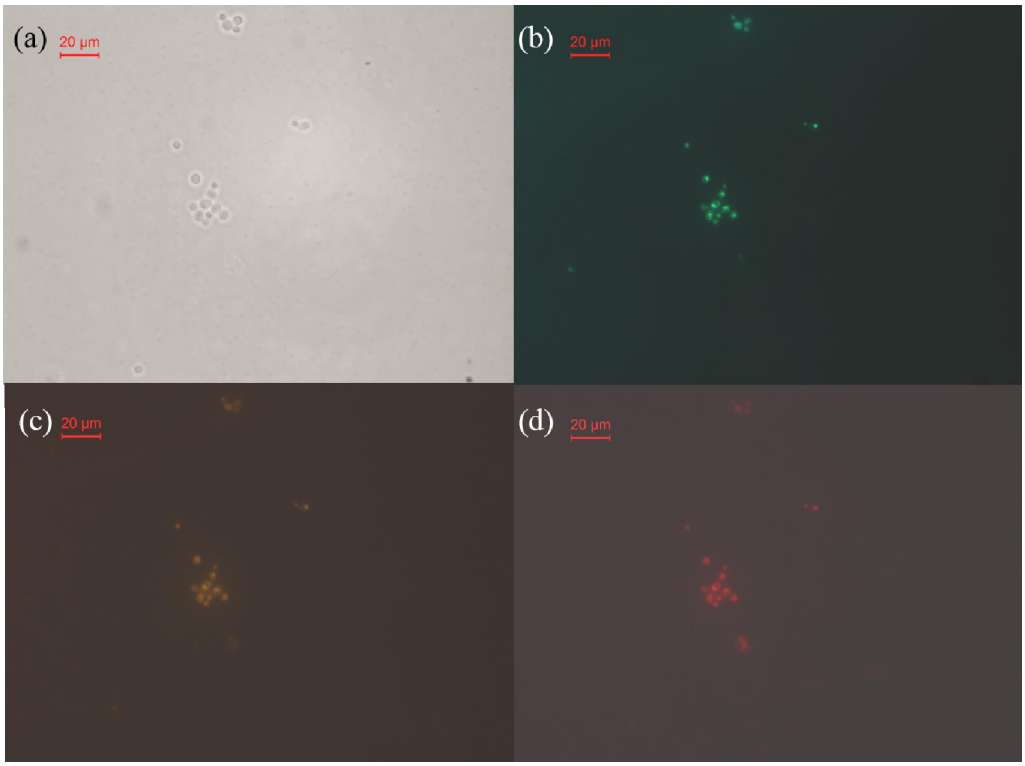

Figure 4.18 *In vitro* bright field and fluorescence images of GSH capped CdS QDs in RAW 264.7 macrophage cells. Images were taken in inverted research microscope under (a) bright field, (b) UV (c) blue and (d) green light

The fluorescence image obtained using UV and blue excitation was exclusively due to quantum dots fluorescence whereas the green light excited fluorescence image also have some fluorescent contribution due to dye. It is seen that even at excitation wavelength between 530-560 nm, the fluorescent pink resorufin dye producing a little fluorescence (**appendix-B**). In the imaging process, UV, blue and green light excitation resulted into green, yellow and red fluorescent images of cells, respectively. This data is corroborating with the luminescence data of the CdS QDs samples. In conclusion, the prepared GSH capped CdS QDs displayed good biocompatibility and fluorescence which makes it a potential candidate for biomedical imaging.

4.7 Conclusion

A facile one-pot polyol approach was used for the synthesis of photo-stable, biocompatible and fluorescing GSH capped CdTe, CdSe and CdS QDs. The microstructural studies of all the three QD systems displayed sharp peaks affirming good crystallinity. The interaction of the functional groups on the QD surface has been studied by the surface analysis. It is observed from the zeta potential studies that all the three QD systems displayed excellent stability at physiological pH making them suitable for biomedical applications. The emission properties were studied with PL and TRPL which showed band-edge type emission for all three systems. Comprehensive toxicity studies of the QD systems are a prerequisite before any biomedical applications. The biocompatibility of GSH capped CdTe, CdSe and CdS QDs were established using the Resazurin Reduction Assay or Alamar Blue (AB) toxicity assay. All the three QD systems exhibited excellent cell viability in RAW 264.7 macrophage cell lines. The QD incubated cells were further investigated under the fluorescent microscope. Due to their efficiency after cellular uptake established themselves as a potential candidate for biomedical imaging. Thus, our findings indicate that the as-prepared CdTe, CdSe, and CdS QDs will have the potential as an alternative probe for *in vivo* imaging and biological tagging.

References:

[1] Rizvi, S. B. *et al.* Semiconductor quantum dots as fluorescent probes for *in vitro* and *in vivo* bio-molecular and cellular imaging. *Nano Rev.* **1,** 1--15, 2010.

[2] Alivisatos, A. P. *et al.* Quantum dots as cellular probes. *Annu. Rev. Biomed. Eng.* 7**,** 55--76, 2005.

[3] Gao, X. *et al*. *In vivo* cancer targeting and imaging with semiconductor quantum dots. *Nat. Biotechnol.* **22** (8)**,** 969--976, 2004.

[4] Smith, A. M. *et al.* Bioconjugated quantum dots for *in vivo* molecular and cellular imaging. *Adv. Drug Delivery Rev.* **60** (11)**,** 1226--1240, 2008.

[5] Walling, M. A. *et al.* Quantum dots for live cell and *in vivo* imaging. *Int. J. of Mol. Sciences* **10** (2)**,** 441--491, 2009.

[6] Pinaud, F. *et al.* Advances in fluorescence imaging with quantum dot bio-probes. *Biomaterials* **27** (9)**,** 1679--1687, 2006.

[7] Shi, L. *et al.* Synthesis and application of quantum dots FRET-based protease sensors. *J. Am. Chem. Soc.* **128** (32)**,** 10378--10379, 2006.

[8] Ballou, B. *et al.* Noninvasive Imaging of Quantum Dots in Mice. *Bioconjug. Chem.* **15** (1)**,** 79--86, 2004.

[9] Vivero-Escoto, J. L. & Huang, Y.T. Inorganic-organic hybrid nanomaterials for therapeutic and diagnostic imaging applications. *Int. J. Mol. Sci.* **12** (6)**,** 3888--3927, 2011.

[10] Barreto, J. A. *et al.* Nanomaterials: Applications in cancer imaging and therapy. *Adv. Mater.* **23** (12)**,** H18--H40, 2011.

[11] Cassidy, P. J. & Radda, G. K. Molecular imaging perspectives. *J. of R. Soc. Interfaces* **2** (3)**,** 133--144, 2005.

[12] Leuschner, F. & Nahrendorf, M. Molecular imaging of coronary atherosclerosis and myocardial infarction: Considerations for the bench and perspectives for the clinic. *Circulation Research* **108** (5)**,** 593--606, 2011.

[13] Cingarapu, S. *et al.* Synthesis of CdSe/ZnS and CdTe/ZnS quantum dots: Refined digestive ripening. *J. of Nanomater.* **2012**,1--12, 2012.

[14] Ung, T. D. T. *et al.* CdTe and CdSe quantum dots: synthesis, characterizations and applications in agriculture. *Adv. Nat. Sci. Nanosci. Nanotechnol.* **3** (4)**,** 043001--043012, 2012.

[15] Talapin, D. V. *et al.* Highly Luminescent Monodisperse CdSe and CdSe/ZnS Nanocrystals Synthesized in a Hexadecylamine-Trioctylphosphine Oxide-Trioctylphospine Mixture. *Nano Lett.* **1** (4)**,** 207--211, 2001.

[16] Qian, H. *et al.* Facile one-pot synthesis of luminescent, water-soluble, and biocompatible glutathione-coated CdTe nanocrystals. *Small* **2** (6)**,** 747--751, 2006.

[17] Gao, M. *et al.* Strongly Photoluminescent CdTe Nanocrystals by Proper Surface Modification. *J. Phys. Chem. B* **102** (43)**,** 8360--8363, 1998.

[18] Ludeke, R. & Paul, W. Growth and Optical Properties of Wurtzite and Sphalerite CdSe Epitaxial Thin Films. *Physica status solidi (b)* **23** (1)**,** 413--418, 1967.

[19] Xue, M. *et al.* The preparation of glutathione-capped CdTe quantum dots and their use in imaging of cells. *Talanta* **83** (5)**,** 1680--1686, 2011.

[20] Liu, Y. F. & Yu, J. S. Selective synthesis of CdTe and high luminescence CdTe/CdS quantum dots: The effect of ligands. *J. Colloid Interface Sci.* **333** (2)**,** 690--698, 2009.

[21] Reis, E. F. dos *et al.* Synthesis and characterization of poly (vinyl alcohol) hydrogels and hybrids for rMPB70 protein adsorption. *Mater. Res.* **9** (2), 185--191, 2006.

[22] Wang, Q. *et al.* Direct synthesis of high-quality water-soluble CdTe:Zn2+ quantum dots. *Inorg. Chem.* **51** (17)**,** 9208--13, 2012.

[23] Zhang, J. *et al.* Aqueous synthesis of ZnSe nanocrystals by using glutathione as ligand: The pH-mediated coordination of Zn2+ with glutathione. *J. Phys. Chem. C* **114** (25)**,** 11087--11091, 2010.

[24] Ferretti, L. *et al.* Glutathione and N-acetylcysteinylglycine: Protonation and Zn2+ complexation. *J. Inorg. Biochem.* **101** (10)**,** 1442--1456, 2007.

[25] Leverrier, P. *et al.* Metal binding to ligands: Cadmium complexes with glutathione revisited. *Anal. Biochem.* **371** (2)**,** 215--228, 2007.

[26] Pu, F. & Ren, J. Lighting up silica nanotubes transcribed from the submicron structure of a metalï peptide hybrid. *Nanotechnology* **24** (37)**,** 375603--375612, 2013.

[27] Han, M. J. *et al.* Determination of configuration of arsenite-glutathione complexes using ECSTM. *Toxicol. Lett.* **175** (1)**,** 57--63, 2007.

[28] Schlegel, G. *et al.* Fluorescence Decay Time of Single Semiconductor Nanocrystals. *Phys. Rev. Lett.* **88** (13), 137401--137404, 2002.

[29] Nirmal, M. *et al.* Observation of the Dark Exciton in CdSe Quantum Dots. *Phys. Rev. Lett.* **75** (20), 3728--3731, 1995.

[30] Vega-Avila, E. & Pugsley, M. K. An overview of colorimetric assay methods used to assess survival or proliferation of mammalian cells. *Proc West Pharmacol. Soc.* **54,** 10--14, 2011.

[31] Bonnier, F. *et al.* Cell viability assessment using the Alamar blue assay: A comparison of 2D and 3D cell culture models. *Toxicol. Vitr.* **29** (1)**,** 124--131, 2015.

[32] Cumming, G. *et al.* Error bars in experimental biology. *J. Cell Biol.* **177** (1)**,** 7--11, 2007.

[33] Xiaofang, S. Encapsulation of CdTe quantum dots in polyvinylpyrrolidone nanoparticle for live cell imaging. *Micro Nano Lett.* **7** (2), 137--141, 2012.

[34] Pu, F. & Ren, J. Lighting up silica nanotubes transcribed from the submicron structure of a metalï peptide hybrid. *Nanotechnology* **24** (37)**,** 375603--375612, 2013.

[35] Hou, J. *et al.* Hydrothermal synthesis of CdS/CdLa2S4 heterostructures for efficient visible-light-driven photocatalytic hydrogen production. *RSC Adv.* **2** (27), 10330--10336, 2012.

[36] Kobayashi, Y. *et al.* Effect of Surface Defects on Auger Recombination in Colloidal CdS Quantum Dots. *J.of Phy. Chem. Let.* **2** (9)**,** 1051--1055, 2011.

[37] Khan, A. CdS nanoparticles with a thermoresponsive polymer: Synthesis and properties. *J. Nanomater.* **2012,** 1--8, 2012.

[38] Li, Y. *et al.* Solvothermal Elemental Direct Reaction to CdE (E = S, Se, Te) Semiconductor Nanorod. *Inorg. Chem.* **38** (7)**,** 1382--1387, 1999.